Chemical Physics 591 (2025) 112578

Contents lists available at ScienceDirect

Chemical Physics

journal homepage: www.elsevier.com/locate/chemphys

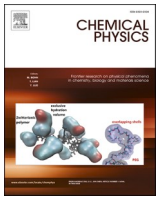

Fundamental physical features of the rhombohedral structure of double perovskite compounds Ba_2NbBO_6 (B = As, Sb, and Bi)

Saber Saad Essaoud [a,b,*], Missoum Radjai [c], Abdelmadjid Bouhemadou [d,**], Mohammed Elamin Ketfi [e], Djamel Allali [f]

[a] Department of Physics, Faculty of Sciences, University of M'sila, University Pole, Road BordjBou-Arreridj, M'sila 28000, Algeria
[b] Laboratory of Materials and Renewable Energy, Faculty of Science, University of M'sila, University Pole, Road Bordj Bou-Arreridj, M'sila 28000, Algeria
[c] Laboratory of Physics of Experimental Techniques and Their Applications (LPTEAM), University of Medea, Algeria
[d] Laboratory for Developing New Materials and Their Characterizations, Department of Physics, Faculty of Science, Ferhat Abbas University - Setif 1, 19000 Setif, Algeria
[e] Department of Electronics, Faculty of Technology, University of M'sila, University Pole, Road Bordj Bou-Arreridj, M'sila 28000, Algeria
[f] University of M'sila, Faculty of Technology, University Pole, Road Bordj Bou-Arreridj, M'sila 28000, Algeria

ARTICLE INFO

Keywords:
Double perovskite
Ab initio calculations
Electronic structure
Charge density topology analysis
QTAIM descriptors
Optical properties

ABSTRACT

This study provides crucial information on the fundamental physical characteristics of Ba_2NbBO_6 (B = As, Sb, and Bi) double perovskites with rhombohedral structure. These compounds are thermodynamically stable in their rhombohedral shape over a pressure range of −20–30 GPa. Electronic structure calculations revealed that Ba_2NbAsO_6, Ba_2NbSbO_6, and Na_2NbBiO_6 are semiconductors with energy bandgaps of 2.101 eV, 1.71 eV, and 2.813 eV, respectively. By analyzing the calculation results from the quantum theory of atoms in molecules, it is expected that the Nb-O and As/Sb/Bi-O bonds to have covalent features. In contract, Ba—O and Ba—As/Sb/Bi bonds exhibit ionic characteristics. We also determined the real and imaginary parts of the dielectric function, absorption coefficient, optical conductivity, loss energy function, reflectivity, refractive index, and extinction coefficient as function of the incident light energy.

1. Introduction

Double perovskites, denoted by the chemical formula $A_2BB'X_6$, are a group of minerals distinguished by the existence of two different cations, B and B′, which occupy the octahedral positions in the crystal lattice. The A-site is usually filled with a monovalent cation, while X denotes an anion, often a halide or oxide that coordinates with the B-site cations. The configuration and characteristics of these materials result in a diverse array of adjustable attributes. Therfore,double perovskite materials are very interesting because they could be used in many fields, including renewable energy, optoelectronics, magnetism, photovoltaics, photocatalysis, transistors, electrochemical energy storage in high-storage capacitors, and mechanical devices [1–6].

The $A_2BB'X_6$ double perovskites have been extensively studied in both experimental and theoretical research. In terms of efficiency, the utilization of $Cs_2AgBiBr_6$, Ba_2FeMoO_6, and $Cs_2AgInCl_6$ compounds in solar cells achieves rates that vary between 5 % and 8 % [7–11]. Although the rates may be lower compared to the efficiency of certain simple perovskites, they exhibit favorable structural and chemical stability. The compounds $Cs_2AgBiBr_6$ and $Cs_2AgInCl_6$havedemonstrated exceptional appropriateness for use in light-emitting devices, achieving a high light-emitting efficiency [12–14]. In experimental conditions, the compound Sr_2CrWO_6 exhibited a significant level of electron mobility, rendering it appropriate for utilization in microelectronic circuits and high-performance transistors [15,16]. Sr_2FeMoO_6 displays diverse resistance when exposed to a magnetic field, along with robust electron mobility and electrical and magnetic properties [17–19]. Two specific double perovskite materials, Ba_2FeMoO_6 and La_2NiMnO_6, have demonstrated a significant response to certain gases such as hydrogen and NO_2. Therefore, these materials have the potential to be used as gas sensors [20,21]. The chemical compositions Sr_2FeMoO_6 and Ba_2BiNbO_6 have been proven to efficiently absorb carbon dioxide, with an efficiency exceeding 15 % [17,22–26]. Essaoud et al. [27] showed that the monoclinic structure of the double perovskite Dy_2CoMnO_6 is a ferromagnetic compound with a consistent total magnetic moment of around $12\mu_B$ within the pressure range of −25–45 GPa. Additionally, this double

* Corresponding author at: Department of Physics, Faculty of Sciences, University of M'sila, University Pole, Road BordjBou-Arreridj, M'sila 28000, Algeria.
** Corresponding author.
E-mail addresses: saber.saadessaoud@univ-msila.dz (S.S. Essaoud), abdelmadjid_bouhemadou@univ-setif.dz (A. Bouhemadou).

https://doi.org/10.1016/j.chemphys.2024.112578
Received 14 October 2024; Received in revised form 8 December 2024; Accepted 10 December 2024
Available online 14 December 2024

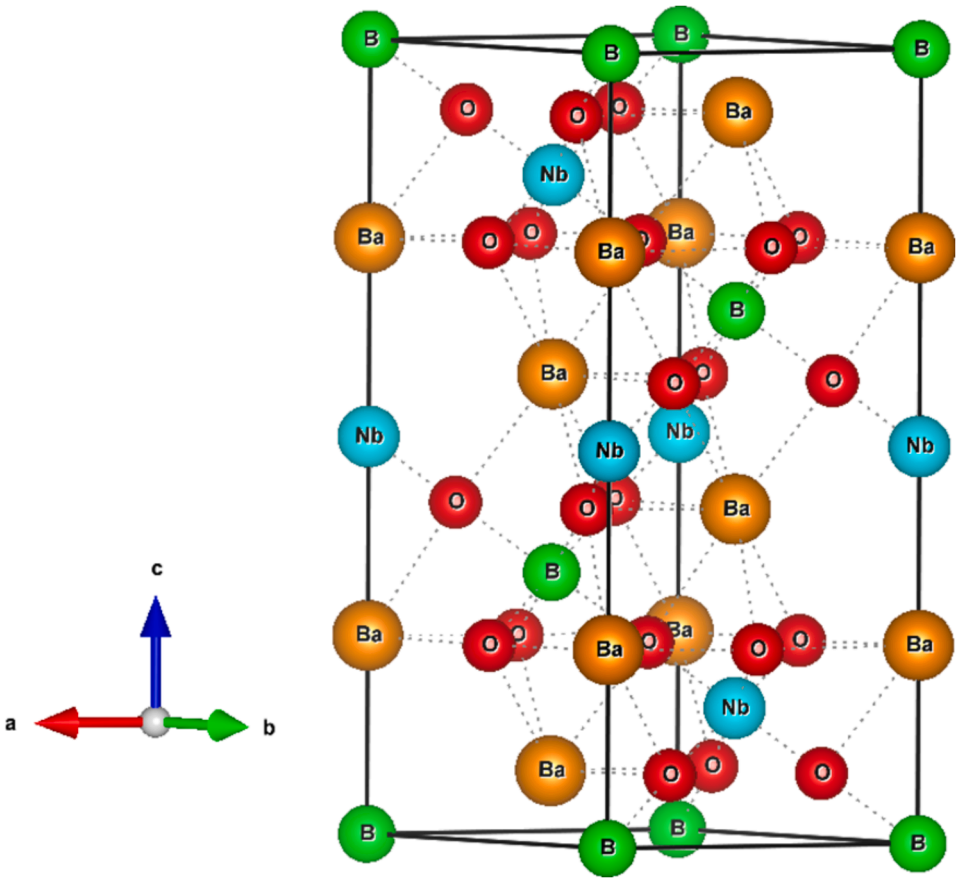

Fig. 1. The rhombohedral structure of double perovskite compounds Ba_2NbBO6 (B = As, Sb and Bi).

perovskite displays semiconductor characteristics in both spin states and shows a high figure of merit (ZT) >0.5 for temperatures above 500 K. Some investigations have been conducted on the magnetic, thermoelectric, optical, mechanical, and thermal properties of halogenated perovskites, including Cs_2AgXBr_6 (X = S, Te, Se) and $X_2AgBiBr_6$ (X = Li, Na, K, Rb, Cs) [28,29]. A theoretical investigation conducted by Assiouan et al.[30]on the compounds Rb_2AuBiX_6 (X = Br, Cl, F) showed that these compounds exhibit significant light absorption (~$5x0^5$ cm^{-1}) and a remarkable reflectivity (~38 %)in the visible region.Studies on the B-site structured Gd_2CuTiO_6 have proven its effectiveness as a basic material used in magnetic cooling. Gd_2CuTiO_6 exhibits good magnetothermal behavior due to the exchange interaction between the Gd-4f and Cu-3d sublattices when the magnetic field is changed by 0–7 T [31]. The maximum change in magnetic entropy ($-\Delta ST_{max}$) of Gd_2CuTiO_6 oxide reaches 51.4 $J{\cdot}kg^{-1}.K^{-1}$ (378.2 $mJ{\cdot}cm^{-3}.K^{-1}$), which is much larger than the commercial magnetic coolant $Gd_3Ga_5O_{12}$, which is 38.3 $J{\cdot}kg^{-1}.K^{-1}$ (271.2 $mJ{\cdot}cm^{-3}.K^{-1}$), and is also superior to most standard cryogenic magnetocaloric material models reported recently [31]. Additionally, other studies have been conducted on oxygenated perovskites such as Ba_2MgReO_6, Ba_2YMoO_6 [32], Ca_2FeMoO_6 [33], Ba_2MnReO_6, Ba_2NiReO_6, and Sr_2MnReO_6 [34], Sr_2TiFeO_6 [27–29] La_2NiMnO_6 [35,36], Ca_2FeMoO_6 [37–39], and Sr_2FeMoO_6 [40–42].

The intriguing results obtained from the studies mentioned above prompted us to conduct this study, which aimed to investigate some fundamental physical properties of the unexplored rhombohedral structure of double perovskite compounds Ba2NbBO6 (B = As, Sb and Bi) using first-principles calculations. This study mainly focuses on the structural stability of the studied compounds in a particular pressure range, as well as the electronic characteristics of these compounds, the nature of the chemical bonds that bind their constituent atoms, and how these compounds react to light incident on them.

2. Calculation settings

The explored physical properties of Ba_2NbBO_6 (B = As, Sb, and Bi) double perovskites in the rhombohedral phase were investigated using two complementing first-principles techniques. The structural properties of the compounds were estimated using the first-principles pseudopotential plane wave method (PP-PW), implemented in the quantum espresso package [43]. The PBEsol version of the generalized gradient approximation (GGA) functional [44] was used to treat the exchange–correlation interactions. In order to obtain precise computations of the structural parameters, a plane wave set with a kinetic energy cutoff of 60 Rydberg was utilized for the wave function developments ($Ecut_{wfc}$) and a cutoff of 480 Rydberg was used for the charge density developments ($Ecut_{rho}$). Additionally, 170 special k-points were employed for the integration over the Brillouin zone (BZ).

The optoelectronic properties were calculated using the full-potential linearised augmented plane wave (FP-LAPW) method, as implemented in the WIEN2k code [45]. The exchange–correlation interactions were modelled using the Tran-Blaha modified Becke-Johnson (TB-mBJ) potential [46]. The threshold value for the plane wave set utilized in generating the function waves in the interstitial space is $R_{MT}K_{max} = 9$, where R_{MT} represents the minimum radius of the Muffin-Tin spheres and K_{max} denotes the maximum wave vector in the reciprocal lattice. The properties of bonds and the effective charge of each atom were analyzed using CRITIC2 [47] and Bader codes [48–50], which are based on the quantum theory of atoms in molecules (QTAIM) [50,51].

Table 1
Computed fractional coordinates of ground state atomic positions, structural parameters (*a* and *c*, in Å), and bulk modulus (*B*, in GPa) for double perovskite compounds. Ba_2NbBO_6 (where B represents As, Sb, and Bi).

	Ba_2NbAsO_6	Ba_2NbSbO_6	Ba_2NbBiO_6
Ba	(0.7502, 0.7502, 0.7502)	(0.7488, 0.7488, 0.7488)	(0.7479, 0. 7479, 0. 7479)
Nb	(0.5, 0.5, 0.5)	(0.5, 0.5, 0.5)	(0.5, 0.5, 0.5)
B	(0, 0, 0)	(0, 0, 0)	(0, 0, 0)
O	(0.7554, 0.7252, 0.2600)	(0.6815, 0.7837, 0.2708)	(0.6693, 0.7894, 0.2761)
a	5.844	6.004	6.076
c	14.293	14.544	14.626
B	160.5	148.4	144.9

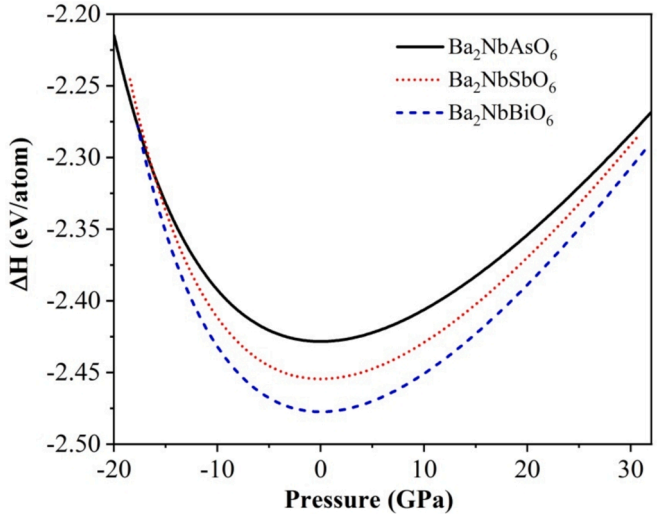

Fig. 2. Variation of formation enthalpy values (ΔH) as a function of pressure for double perovskite compounds Ba_2NbBO_6 (B = As, Sb and Bi).

3. Results and discussion

3.1. Structural characteristics

A unit cell of the rhombohedral structure of Ba_2NbBO_6 (B = As, Sb, and Bi) double perovskite compounds is displayed in Fig. 1. The estimated equilibrium structural parameters, including the lattice parameters (*a* and*c*) and atomic position coordinates as well as the bulk modulus B are listed in Table 1.The data provided in this table show that all three of the compounds under investigation have good ability to withstand the change in volume resulting from the effect of external pressure (see Fig. 2).

The enthalpy of formation (ΔH_{for}) was determined within a pressure range of −20–30 GPa using the following expression:

$$\Delta H_{for} = \frac{E_{tot}^{Ba_2NbBO_6} - (n_{Ba}E_{solid}^{Ba} + n_B E_{solid}^{B} + n_{Nb}E_{solid}^{Nb} + n_O E_{Gas}^{O})}{n_{Ba} + n_B + n_{Nb} + n_O}$$

In this context, $E_{tot}^{Ba_2NbBO_6}$ represents the total energy of an unit cell of the compound Ba_2NbBO_6, E_{solid}^{Ba}, E_{solid}^{B}, and E_{solid}^{Nb} denote the total energies per atom of the solid form of the pure elements Ba, B (As/Sb/Bi)and Nb respectively, and E_{Gas}^{O} denotes the total energy per atom of the gaseous state of the oxygen atom. The curves showing the enthalpy of formation (ΔH_{for}) as a function of pressure ($\Delta H_{for}(P)$) indicate that all three compounds are very stable since they have negative enthalpies of formation in the pressure range from −20 to 30 GPa. Moreover, the relation:$\Delta H_{Ba_2NbBiO_6} > \Delta H_{Ba_2NbSbO_6} > \Delta H_{Ba_2NbAsO_6}$ indicates the influence of the B atom's characteristics on thermodynamic stability – the thermodynamic stability increases when arsenic (As) is substituted with antimony (Sb) and when antimony (Sb) is substituted with bismuth (Bi).

We analysed the phonon dispersion spectra of the compounds under study to evaluate their dynamical stability. This study used the finite displacement method as implemented in the CASTEP code [52]. Figure F3 illustrates the resulting phonon dispersion diagrams for the considered materials. Fig. 3 demonstrates the presence of soft modes (also called imaginary modes, characterised by negative frequencies) in the studied compounds. Theoretically, materials are considered dynamically stable when their phonon dispersion contains no soft modes and dynamically unstable when they do. These soft modes are recognised for triggering lattice instability, which may result in structural phase transitions. Furthermore, their presence may indicate that synthesising the compound under standard conditions could be difficult. It is essential to highlight the complex implications arising from negative frequencies in the phonon dispersion curves of materials. In certain instances, presence of soft modes in the phonon dispersion curve of a material does not definitively indicate that the crystal structure of this material possess an intrinsic instability. Many stable synthesised materials exhibit soft vibrational modes [53], which demonstrate that a material can maintain dynamic stability despite these soft modes. Consequently, soft modes in the materials Ba_2NbAsO_6, Ba_2NbSbO_6, and Ba_2NbBiO_6 should not be hastily construed as evidence against the feasibility of their synthesis. Further research is needed to determine the prerequisites for the synthesis and stabilization of the materials concerned.

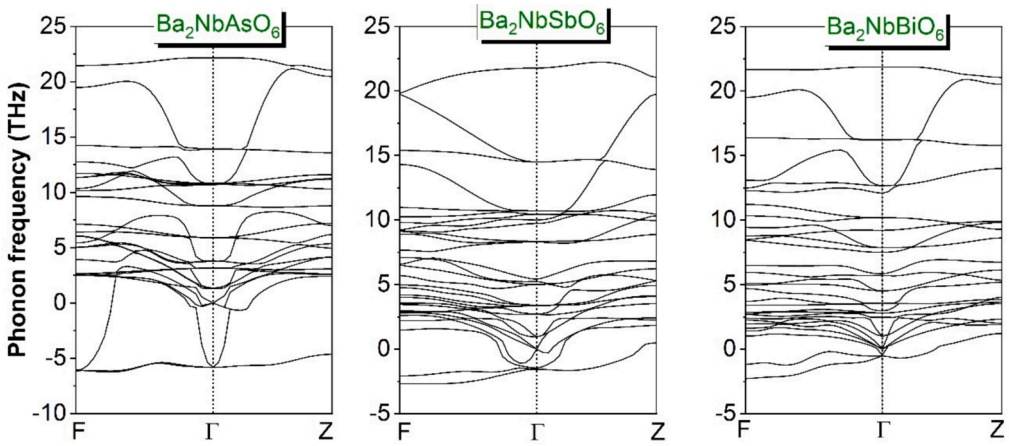

Fig. 3. Phonon dispersion spectra for for double perovskite compounds Ba_2NbAsO_6, Ba_2NbSbO_6, and Ba_2NbBiO_6.

Table 2
The calculated effective charge (Q^{eff}), distance between the nucleus of the atom and the nearest critical point (d_{N-CP}, in Å), and total volume of the Bader region (Ω_{Bader}, in Å^3) for the constituent atoms of double perovskite compounds Ba_2NbBO_6 (B = As, Sb and Bi).

$Ba_2NbAsO6$				Ba_2NbSbO_6			Ba_2NbBiO_6		
Atom	Q^{eff}	d_{N-CP}	Ω_{Bader}	Q^{eff}	d_{N-CP}	Ω_{Bader}	Q^{eff}	d_{N-CP}	Ω_{Bader}
B	+1.646	1.761	76.517	+1.817	1.953	102.983	+1.837	2.088	115.159
Ba	+1.574	2.695	147.020	+1.564	2.554	153.002	+1.599	2.552	155.634
Ba	+1.573	2.692	146.978	+1.563	2.554	152.945	+1.598	2.551	155.622
Nb	+2.660	1.706	61.688	+2.674	1.715	62.419	+2.694	1.702	62.616
O	−1.24	1.523	86.447	−1.269	1.596	91.772	−1.274	1.604	93.741

Table 3
Difference in electro-negativity ($\Delta\eta$) and distance (d, in Å) between the constituent atoms of double perovskite compoundsBa_2NbBO_6(B=As, Sb and Bi).

Electro-negativity difference	Ba_2NbAsO_6	Ba_2NbSbO_6	Ba_2NbBiO_6
$\Delta\eta_{O-As} = 1.26$	$d_{(O\text{-}As)}$ = 2.14665 Å	$d_{(O\text{-}Sb)}$ = 2.28298 Å	$d_{(O\text{-}Bi)}$ = 2.34135 Å
$\Delta\eta_{O-Sb} = 1.39$			
$\Delta\eta_{O-Bi} = 1.47$	$d_{(O\text{-}Ba1)}$ = 2.92152 Å	$d_{(O\text{-}Ba1)}$ = 3.03449 Å	$d_{(O\text{-}Ba1)}$ = 2.96909 Å
$\Delta\eta_{O-Ba} = 2.55$	$d_{(O\text{-}Ba2)}$ = 3.01140 Å	$d_{(O\text{-}Ba2)}$ = 2.69968 Å	$d_{(O\text{-}Ba2)}$ = 2.68018 Å
$\Delta\eta_{O-Nb} = 1.84$	$d_{(O\text{-}Nb)}$ = 1.98743 Å	$d_{(O\text{-}Nb)}$ = 1.99157 Å	$d_{(O\text{-}Nb)}$ = 1.99304 Å

3.2. Chemical bonding nature

Examining and analyzing the nature of bonding in compounds is essential due to its relationship with the material's hardness and other fundamental physical properties. In this context, the quantum theory of atoms in molecules (QTAIM) [50,51], integrated into the Bader [48,50] and CRITIC2 [47] programs, was employed to evaluate the characteristics of atomic bonds at the bond's critical point (BCP), utilizing the topology of the charge distribution within the crystal space between atoms.

The effective charge (Q^{eff}) values of the constituent atoms in Ba_2NbBO_6 (B = As, Sb, and Bi), presented in Table 2, were computed using Bader software. The effective charge of an atom in a molecule is calculated as the difference between the atomic number (Z) and the Bader charge (Q^{Bader}), which is the number of electrons in the Bader area (Ω): $Q^{eff} = Z - Q^{Bader} = Z - \int_{\Omega} \rho(r)dr$, where ρ(r)denotes the electron density at a location defined by the vector position ***r*** within Bader's area (Ω). The Bader area of an atom is delineated between its nucleus and the critical regions. The critical points (CP) arelocations where the electron density gradient is zero; $\nabla\rho(r) = 0$, indicating the absence of the electric field generated by positive nuclei acting on negative charges. The critical points are the positions between atoms where electrons experience balanced attractive forces from the nuclei of adjacent atoms; they represent the limits of atomic effect on the charges present in their vicinity. From Table 2, the data obtained imply a transfer of electric charges from the atoms Ba, Nb, and As/Sb/Bi to the oxygen atom. An additional finding from these data indicates that the transferred charge levels are not precisely integers, implying that the bond type may be a mixture of ionic and covalent. The principal factors affecting charge transfer between atoms are their interatomic distance and electronegativity difference. Table 3 presents the values of the distance and electronegativity difference between the atoms Ba, Nb, As/Sb/Bi, and the oxygen atom. The results indicate that the interatomic distance exerts the most significant effect on charge transfer, with the largest charge migrating from the Nb atom to the oxygen atom due to this distance being less than 2 Å and the shortest compared to other interatomic

Table 4
Topological and QTAIM descriptors at the bond critical points (BCP) for Ba_2NbBO_6 (B = As, Sb and Bi) compounds calculated with including spin–orbit coupling (Full relativistic). E1 and E2 are the bond ends. r_1 (in Å) is the distance from the first atom (E1) to the BCP, and r_2 is the distance from the second atom (E2) to the BCP.$\widehat{\alpha}$ = E1 - BCP - E2 is the angle between the two atoms (E1 and E2) and the BCP. ρ_b is the electron density (in e.Å^{-3} unit). $\nabla^2\rho_b$ is the Laplacian of the electron density (in e. Å^{-5} unit). $\boldsymbol{V_b}$ is the potential electronic energy density (in *a.u* unit). $\boldsymbol{G_b}$ is the kinetic electronic energy density (in *a.u* unit). $\boldsymbol{H_b}$ is the density of the total electronic energy (in *a.u* unit).

System	Bond (E1-E2)	BCP coordinates			QTAIM descriptors									
		x	*y*	*z*	r_1	r_2	r_1/r_2	$\widehat{\alpha}$	ρ_b	$\nabla^2\rho_b$	G_b	V_b	$\lvert V_b\rvert/G_b$	H_b
Ba_2NbAsO_6	Nb—O	0.623	0.369	0.640	1.704	2.052	0.830	179.990	0.114	0.510	0.162	−0.197	1.215	−0.035
	As—O	0.143	0.865	0.127	2.105	1.952	1.078	179.980	0.074	0.170	0.066	−0.090	1.358	−0.024
	Ba—O	0.025	0.491	0.742	2.949	2.409	1.224	178.190	0.024	0.081	0.019	−0.018	0.943	0.001
	Ba—O	0.034	0.749	0.733	3.028	2.494	1.214	177.440	0.021	0.067	0.016	−0.015	0.936	0.001
	Ba—O	0.749	0.733	0.485	3.028	2.494	1.214	177.390	0.021	0.066	0.016	−0.015	0.936	0.001
	Ba—O	0.262	0.520	0.957	3.110	2.584	1.204	176.020	0.018	0.054	0.013	−0.012	0.935	0.001
	Ba—As	0.128	0.128	0.128	3.303	3.444	0.959	180.000	0.015	0.033	0.008	−0.008	0.992	0.000
Ba_2NbSbO_6	Na—O	0.401	0.345	0.625	1.708	2.056	0.831	179.960	0.113	0.505	0.160	−0.194	1.211	−0.034
	Sb—O	0.171	0.116	0.855	2.310	2.005	1.152	179.920	0.066	0.167	0.058	−0.075	1.285	−0.017
	Ba—O	0.737	0.511	0.008	2.279	2.823	0.807	179.530	0.030	0.110	0.027	−0.025	0.961	0.001
	Ba—O	0.763	0.490	0.710	3.067	2.534	1.211	177.810	0.019	0.060	0.014	−0.013	0.929	0.001
	Ba—O	0.289	0.238	0.963	3.132	2.604	1.203	177.570	0.017	0.051	0.012	−0.011	0.925	0.001
	Ba—Sb	0.869	0.869	0.869	3.592	3.310	1.085	180.000	0.015	0.029	0.007	−0.008	1.020	0.000
Ba_2NbBiO_6	Nb—O	0.342	0.622	0.408	2.057	1.709	1.204	179.960	0.112	0.503	0.159	−0.192	1.209	−0.033
	Bi—O	0.884	0.152	0.818	2.434	1.990	1.223	179.890	0.064	0.194	0.061	−0.075	1.213	−0.013
	Ba—O	0.005	0.734	0.517	2.805	2.260	1.241	179.670	0.031	0.115	0.028	−0.027	0.964	0.001
	Ba—O	0.703	0.765	0.493	3.073	2.539	1.210	177.600	0.019	0.059	0.014	−0.013	0.927	0.001
	Ba—O	0.040	0.705	0.763	2.657	3.183	0.835	177.110	0.016	0.045	0.010	−0.010	0.922	0.001
	Ba—Bi	0.868	0.868	0.868	3.332	3.636	0.916	180.000	0.014	0.027	0.007	−0.007	1.020	0.000

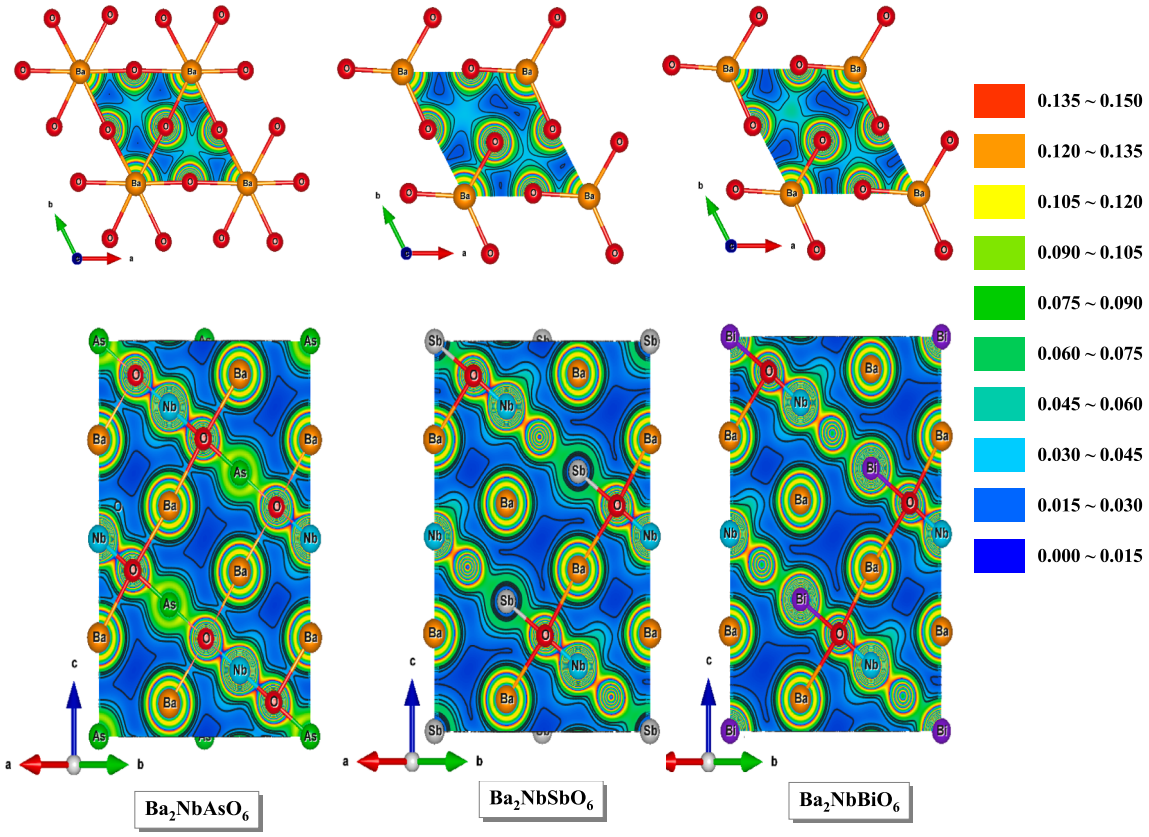

Fig. 4. The electron charge density distribution map ofdouble perovskite compounds Ba_2NbAsO_6, $Ba_2NbBSbO_6$, and Ba_2NbBiO_6.

distances. This occurs despite the electronegativity difference of 1.84 between Nb and O($\Delta\eta_{O-Nb} = 1.84$), while the electronegativity difference between the oxygen and barium atoms is the most significant ($\Delta\eta_{O-Ba} = 2.55$). Taking into account the distance between the atomic nucleus and the nearest critical point ($d_{N\text{-}CP}$), as well as the total volume of the Bader region (Ω_{Bader}) for the constituent atoms of the Ba_2NbBO_6 (B = As, Sb, and Bi) double perovskite compounds, the results indicate that the vicinity surrounding the Ba atoms exhibits a low electron density.

To validate the findings concerning the transfer of charge from anions to cations and to elucidate the characteristics of the bonds between them, we analyzed the Attractor connectivity matrix for each compound and descriptors of the QRAIM at the bond critical points (BCP) using the CRITIC2 program. The calculated values are presented in Table 4.

The attractor connectivity matrix aids in determining the interaction frequency of each atom with other atoms in the compound. The Attractor connectivity matrix values for the three compounds indicate that the oxygen atom exhibits a stronger interaction with the barium atom, while interacting to a lesser and equal degree with the Nb and As/Sb/Bi atoms.

As	**Ba**	**Nb**	**O**	
As	0	2	0	6
Ba	1	0	0	12
Nb	0	0	0	6
O	1	4	1	0

Sb	**Ba**	**Nb**	O	
Sb	0	2	0	6
Ba	1	0	0	9
Nb	0	0	0	6
O	1	3	1	0

Bi	**Ba**	**Nb**	**O**	
Bi	0	2	0	6
Ba	1	0	0	9
Nb	0	0	0	6
O	1	3	1	0

Attractor connectivity matrix

The primary descriptor employed to determine the bond type is the charge density at the critical points (BCP). The charge density data indicate that the bonds As—Ba, Sb—Ba, Bi—Ba, and Ba—O exhibit low charge density, whereas the bonds Nb—O, As—O, Sb—O, and Bi—O demonstrate significantly higher electron density. Fig. 4 shows the charge density distribution among the atoms. The charge density values found are consistent with the information in Table 4.

Although the values of charge density in the bonds are known, the critical parameters for determining and comprehending the nature of the bond include the kinetic electronic energy density (G_b), potential electronic energy density (V_b), and total electronic energy density (H_b), which are defined as follows:

$$V_b(r) = \frac{1}{2}\int \frac{\rho(r')}{|r-r'|}dr'$$

$$G_b(r) = \frac{1}{2}\sum_{i}^{occupied} |\nabla\psi_i(r)|^2$$

$$H_b = V_b + G_b$$

$$\frac{1}{4}\nabla^2\rho_b(r) = V_b(r) + 2G_b(r)$$

In this context, ρ(r) represents the electron charge density at a point defined by the position vector $\boldsymbol{r}$, $\psi_i(r)$ denotes the orbital wave functions of the occupied electrons at the point $\boldsymbol{r}$, and $\nabla\psi_i(r)$ signifies the spatial gradient of these functions.

Numerous sources examining atomic bond characteristics indicate that QTAIM descriptors can be utilized to ascertain the nature of these bonds. An ionic bond is defined by a reduction of local charges along the essential band path. The ionic bond is distinguished by certain QTAIM descriptors: a low electron density (ρ_b) at the BCP, a positive Laplacian of the electron density ($\nabla^2\rho_b > 0$), a positive density of the total electronic energy ($H_b > 0$) and a negative potential electronic energy density ($V_b < 0$) with an absolute value comparable to the kinetic electronic energy density (G_b); $|V|_b \approx G_b$. A covalent bond is generated through the accumulation of localized charges. A covalent bond is characterized by elevated electron density (ρ_b) at the BCP, a positive Laplacian of the

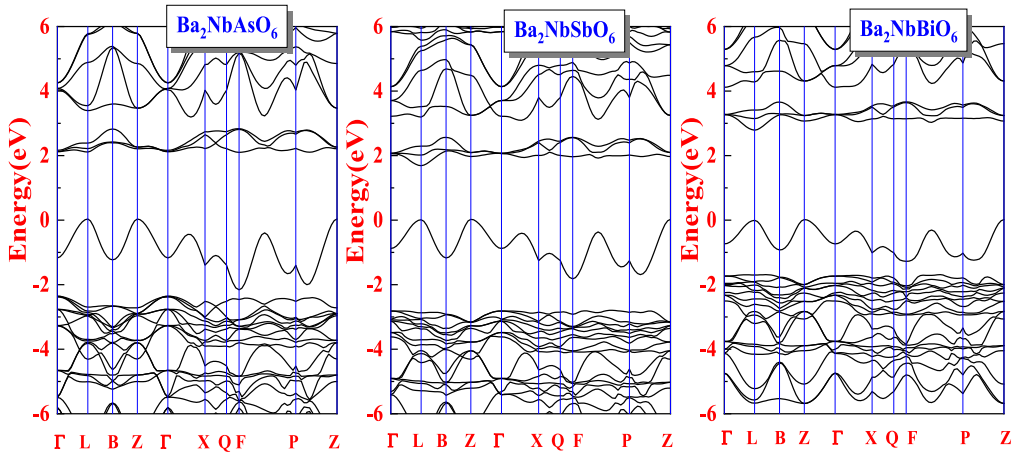

Fig. 5. Band structure spectra for the double perovskite compounds Ba_2NbAsO_6, Ba_2NbSbO_6 and Na_2NbBiO_6 calculated using the TB-mBJ potential.

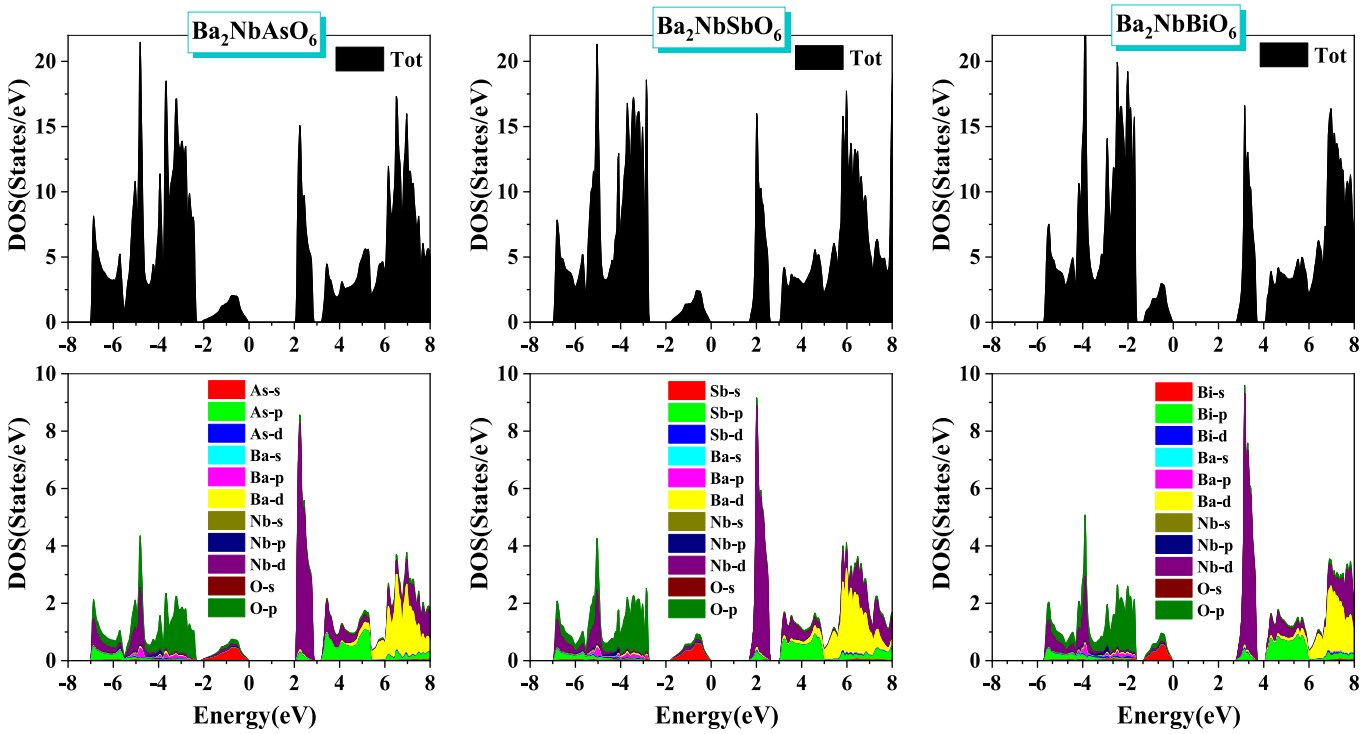

Fig. 6. Total density of states (TDOS) and partial density of states (PDOS) curves for double perovskite compounds Ba_2NbAsO_6, Ba_2NbSbO_6 and Na_2NbBiO_6 calculated using the TB-mBJ potential.

electron density ($\nabla^2\rho_b < 0$), a negligible density of the total electronic energy ($H_b \ll 0$), a negative potential electronic energy density ($V_b < 0$) with a substantially lower absolute value compared to kinetic electronic energy density ($|V_b| \gg G_b$) [54–56].

The analysis of the QTAIM descriptors presented in Table 4 reveals that the Nb—O, As—O, Sb—O, and Bi—O bonds are covalent ($V_b > G_b$, and $H_b < 0$), whereas the Ba—O, Ba—As, Ba—Sb, and Ba—Bi bonds are of ionic nature ($H_b > 0$, and $\frac{|V_b|}{G_b} \approx 1$).

Furthermore, the ratio $R = r_1/r_2$, where r_1 represents the distance from the first atom (E1) of the bond to the critical point (BCP), and r_2 denotes the distance from the second atom (E2) of the bond to the identical critical point, can be used to characterize the charge distribution in the bond (E1-E2). If the ratio $R = r_1/r_2$ exceeds one, it indicates that the critical point of the bond is nearer to atom E2, signifying that the charge density in the region between the critical point and atom E2 along the bond is greater than that in the region between the critical point and atom 1.

The angle between the two atoms (E1 and E2) and the bond critical point (BCP) provides insights into the spatial geometry of molecular bonds. An angle of 180 degrees indicates that the critical point is positioned in a straight line between the two atoms, signifying a linear bond. If its value deviates from 180 degrees, this signifies that the critical point does not align perfectly in a straight line between the two atoms, indicating a non-linear bond. Our observations (shown in Table 4) indicate that all bonds in the compounds are linear, with the exception of the Ba—O link, which is nonlinear.

3.3. Electronic structure

Fig. 5 shows the energy band dispersions of the double perovskites Ba_2NbAsO_6, Ba_2NbSbO_6 and Na_2NbBiO_6along the high symmetry lines

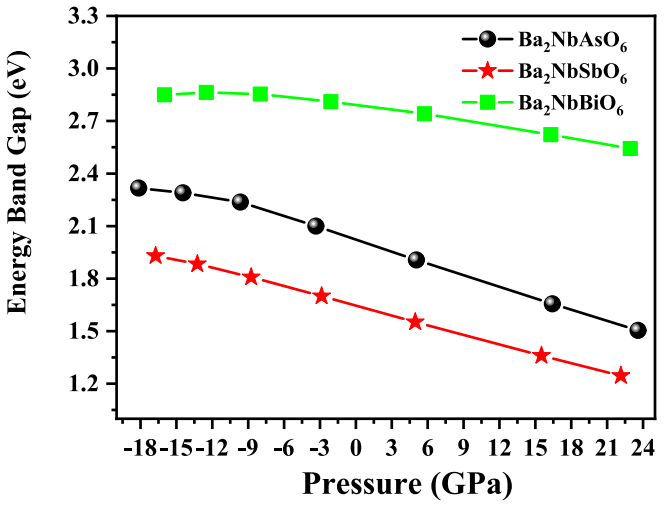

Fig. 7. Pressure dependence of the energy band gap of Ba_2NbAsO_6, Ba_2NbSbO_6 and Na_2NbBiO_6compounds.

calculated using the FP-LAPW method with the TB-mBJ potential. Fig. 5 highlights that the three compounds have semiconducting behavior with an indirect bandgap (L-Z). Ba_2NbSbO_6 has the lowest bandgap value (1.7 eV), Na_2NbBiO_6 has the highest bandgap value (2.81 eV), and Ba_2NbAsO_6has an intermediate band gap value (2.1 eV). These bandgap values are close to those of materials used in photovoltaic devices.

The analysis of total density of states (TDOS) and *l*-decomposed atom-projection density of states (PDOS) curves facilitates the prediction of the electrical conductivity characteristics (conductor, insulator, or semiconductor) of materials. It also enables the identification of the origins of electronic orbitals within the energy bands, particularly those involved in chemical bonding (valence electrons beneath the Fermi level) and those responsible for conduction and charge transfer (conduction electrons above the Fermi level).

Fig. 6 illustrates the total density of states (TDOS) and partial density of states (PDOS) curves for the compounds Ba_2NbAsO_6, Ba_2NbSbO_6, and Na_2NbBiO_6, computed using the Tran-Blaha modified Becke-Johnson (TB-mBJ) potential. The TDOS curves indicate the absence of electronic states inside the barrier bands of 2.101 eV for Ba_2NbAsO_6, 1.71 eV for Ba_2NbAsO_6, and 2.813 eV for Na_2NbBiO_6, respectively. This validates the semiconductor properties of the examined substances. The examination of the PDOS curves for the three compounds indicates that the *d* orbitals of the Nb atoms significantly contribute to the creation of the conduction band in the energy ranges of 2.0–3.0 eV for Ba_2NbAsO_6, 1.9–3.0 eV for Ba_2NbSbO_6, and 2.8–3.5 eV for Ba_2NbBiO_6. The *d* orbitals of Nb atoms, *p* orbitals of Bi atoms, and *d* orbitals of Ba atoms contribute to the conduction band with energies exceeding 3.5 eV. The valence band, spanning from −2.0 eV to the Fermi level, comprises the *s* orbitals of As/Sb/Bi atoms, while the *p* orbitals of O atoms and the *d* orbitals of Nb atoms constitute the valence band stretching from −7.0 to −3.5 eV.

Besides the impact of the B atom's characteristics in the double perovskite compounds Ba_2NbBO_6 (B = As, Sb, and Bi) on the energy gap value, we evaluated the effects of applied pressure within a range of −20–20 GPaon the energy band gap. Fig. 7 illustrates that the application of pressure to the Ba_2NbBO_6 compounds (where B = As, Sb, and Bi) results in a reduction in the energy gap value. The band gap value diminishes linearly with increasing pressure, attributable to the reduction of atomic distances induced by the applied pressure, resulting in altered

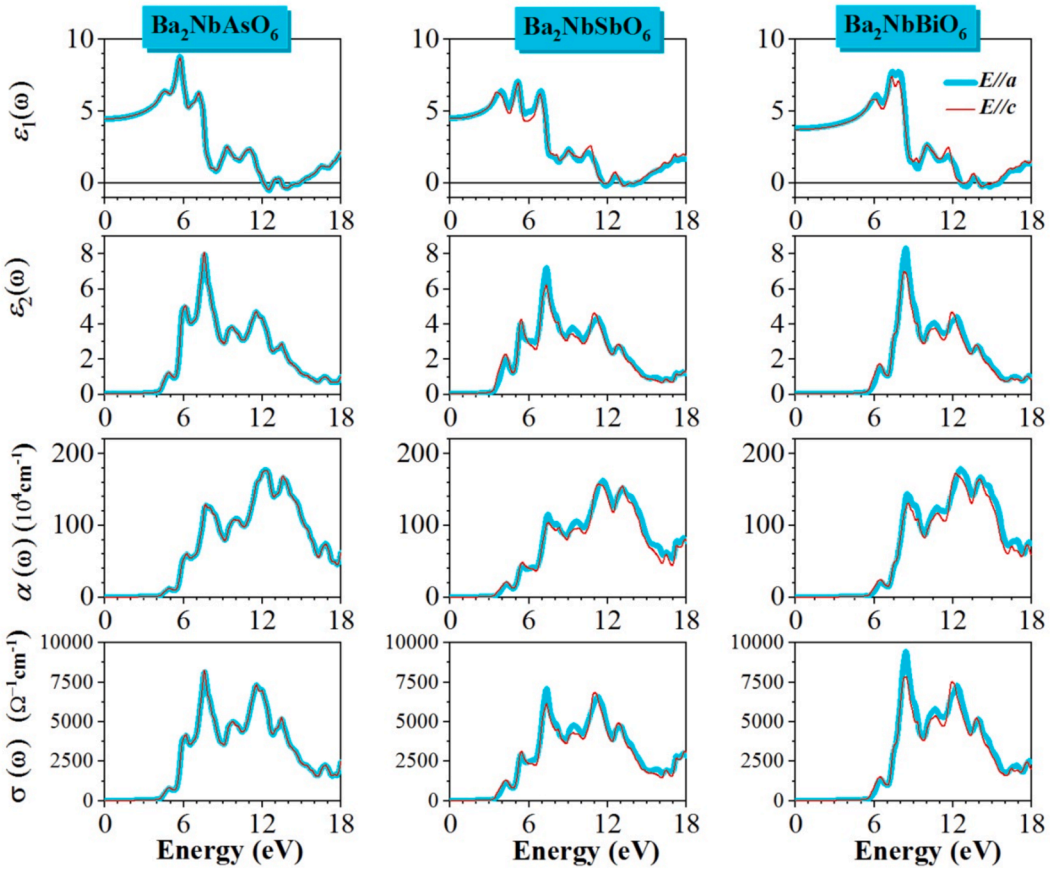

Fig. 8. Real and imaginary parts ($\varepsilon_1(\omega)$, and $\varepsilon_2(\omega)$) of the dielectric function, absorptioncoefficient $\alpha(\omega)$and optical conductivity$\sigma(\omega)$forBa_2NbBO_6 (X = As, Sb and Bi).

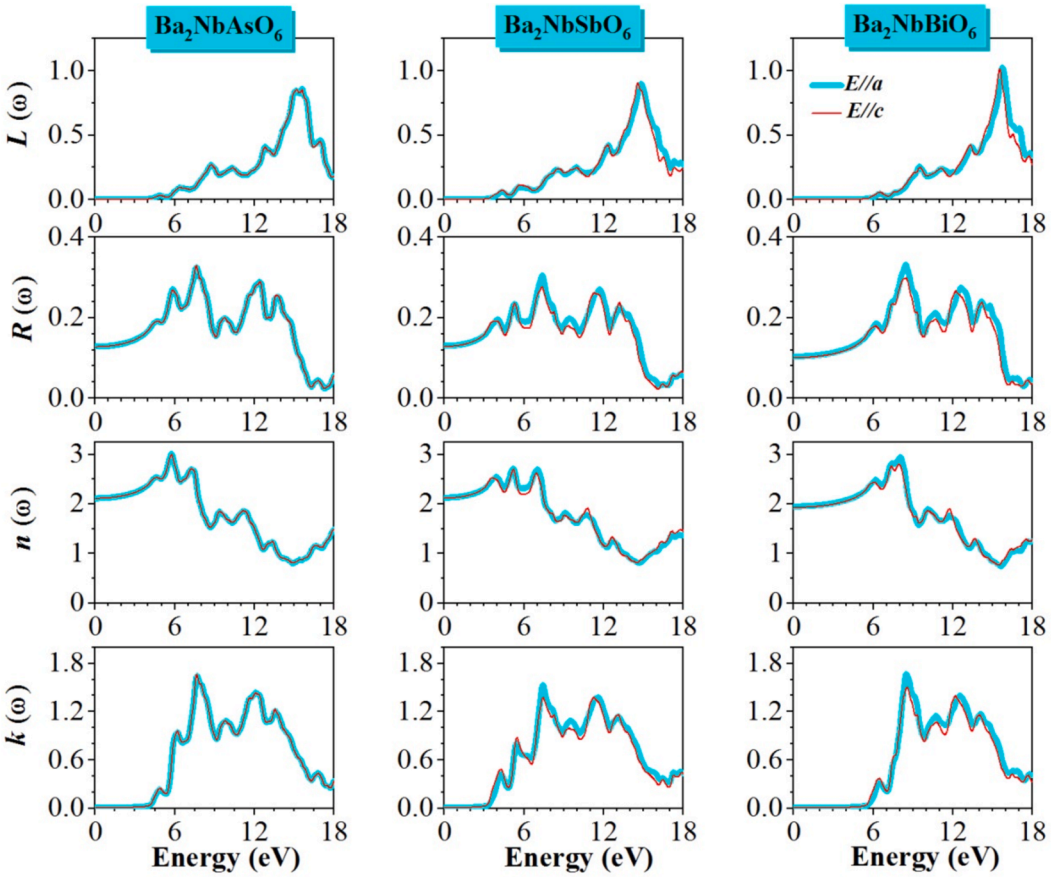

Fig. 9. The calculated spectra of the loss energy $L(\omega)$,reflectivity $R(\omega)$,refractive index $n(\omega)$, and extinction coefficient $k(\omega)$for Ba_2NbBO_6 (B = As, Sb and Bi).

interatomic potential.

3.4. Optical characteristics

Comprehending the optical characteristics of substances provides essential insights into their interactions with light, hence enhancing our understanding of their potential uses in optoelectronic devices. To effectively utilize materials in optoelectronic devices including solar cells, lasers, energy storage systems, and diodes, a comprehensive understanding of their optical properties is essential. This study systematically examines the optical characteristics of Ba_2NbBO_6 (B = As, Sb, and Bi) utilizing the FP-LAPW method with the TB-mBJ potential. The linear optical functions of the considered materials were calculated for two polarizations of the electric field vector of the incident electromagnetic waves ($\vec{E}$) along two major crystallographic directions ($\vec{E}$//[1 0 0] and $\vec{E}$//[0 0 1]) throughout the energy range of 0–18 eV.

The complex dielectric function $\varepsilon(\omega)(\varepsilon(\omega) = \varepsilon_1(\omega) + i\varepsilon_2(\omega))$ characterizes a medium's response to incident electromagnetic radiation. The real part of the dielectric function ($\varepsilon_1(\omega)$)denotes the dispersion of electromagnetic radiation within the material, whereas the imaginary part of the dielectric function ($\varepsilon_2(\omega)$) signifies the absorption of electromagnetic radiation by the substance. The optical functions characterizing the optical characteristics of material can be obtained from the complex dielectric function through established connections [57–59]. The spectra of the real and imaginary components of the dielectric function ($\varepsilon_1(\omega)$, and $\varepsilon_2(\omega)$) for incident electromagnetic waves polarized along the [1 0 0] and [0 0 1] crystallographic directions were calculated using the optical properties computational package in the WIEN2k code, with the results displayed in Fig. 8. The plasma frequency is the limit above which materials demonstrate dielectric characteristics ($\varepsilon_1 > 0$), and below which they exhibit metallic qualities ($\varepsilon_1 < 0$) [60].

The static dielectric function ($\varepsilon(0)$), equivalent to $\varepsilon_1(\omega\rightarrow 0)$, is measured 4.4 for Ba_2NbAsO_6, 4.6 for Ba_2NbSbO_6, and 3.9 for Ba_2NbBiO_6. $\varepsilon(0)$ is a crucial optical parameter that is inversely related to the energy bandgap value [61], which is 2.101 eV for Ba_2NbAsO_6, 1.710 eV for Ba_2NbSbO_6, and 2.813 eV for Ba_2NbBiO_6. Fig. 6 demonstrates that the curve of $\varepsilon_1(\omega)$ ascends from its initial value $\varepsilon_1(\omega\rightarrow 0)$, attaining a maximum of 9 at 5 eV for Ba_2NbAsO_6, 7 at 5.1 eV for Ba_2NbSbO_6, and 7.8 at 7 eV for Ba_2NbBiO_6. Within the energy ranges of 12–13 eV and 13.5–14.5 eV, the examined compounds Ba_2NbBO_6 (where B = As, Sb, and Bi) exhibit negative values, decreasing to about −1 for all three compounds. Within this frequency range, the compounds demonstrate metallic characteristics, exhibiting low light transmission and high reflection [62].

Fig. 8 shows that the spectra $\varepsilon_2(\omega)$ for the two polarizations of the incident electromagnetic radiations have nearly identical shapes for Ba_2NbBO_6 (B = As, Sb, and Bi) compounds, indicating the isotropy of the optical properties of the considered materials. Some differences emerge around 7.5 eV where the main peaks for $\vec{E}\|a$ and $\vec{E}\|c$ for Ba_2NbSbO_6 and $Ba_2NbBiO_6$are slightly shifted. The semiconductors Ba_2NbBO_6 (B = As, Sb, and Bi) are characterized by a rapid increase of the B curves around 4.0 eV, which likely is due to transitions between more distant energy bands.

The spectra of the absorption coefficient $\alpha(\omega)$ are also illustrated in Fig. 8. The $\alpha(\omega)$ curve exhibits a steep ascent from the absorption threshold to around 5 eV, thereafter maintaining a somewhat stable level up to 7.5 eV. Within the 8–9 eV region, the $\alpha(\omega)$ spectrum exhibits a minor decrease prior to an increase, culminating in a peak value of $175 \times 10^4 cm^{-1}$ at 12 eV. This highest value of the absorption coefficient is a little lower than the highest value of the absorption coefficient in simple perovskite compounds such as $BaHfO_3$ [63].

Fig. 9 illustrates the energy loss function $L(\omega)$, reflectivity $R(\omega)$,

refractive index $n(\omega)$, and extinction coefficient $k(\omega)$ throughout a broad photon energy spectrum for the three compounds Ba_2NbBO_6, where B = As, Sb, and Bi. The $R(\omega)$ values do not converge to unity as energy approaches zero, signifying that these compounds demonstrate semiconducting characteristics. We note that the maximum values of the reflectivity coefficient of the studied double perovskite compounds are close to the maximum values of some simple perovskite compounds such as $CsPbX_3$ (X = Br, Cl and I) [63].

The electron energy loss function $L(\omega)$ is an essential metric that characterizesthe energy loss of a high-velocity electron traversing a material. Peaks in the $L(\omega)$ spectra are related to plasma resonance, with the accompanying frequency referred to as the plasma frequency ω_P. The maxima in $L(\omega)$ align with the trailing edges of the reflection spectra; for instance, the peak of $L(\omega)$ for Ba_2NbBO_6 (B = As, Sb, and Bi) is observed at approximately 15 eV, coinciding with the sharp decline in the $R(\omega)$ curve. The static refractive index $n(\omega)$ values are as follows: $n(0) = 2.13$ for Ba_2NbSbO_6, 2.09 for Ba_2NbBiO_6, and 1.95 for Ba_2NbAsO_6. The extinction coefficient, $k(\omega)$(the imaginary component of the complex refractive index) exhibits a pronounced peak at approximately 8 eV.

4. Conclusion

This study employed first-principles computational methods to examine the structural, electronic, and optical properties of the compounds Ba_2NbAsO_6, Ba_2NbSbO_6, and Ba_2NbBiO_6. The findings disclose substantial information regarding these compounds and their properties. These compounds exhibit exceptional structural stability under pressures up to 30 GPa. Ba_2NbAsO_6, Ba_2NbSbO_6, and Na_2NbBiO_6 demonstrate semiconductor properties, with band gap values of 2.101 eV, 1.71 eV, and 2.813 eV, respectively. Moreover, through the application of the quantum theory of atoms in molecules (QTAIM), we analysed the charge density distribution among atoms, alongside the computation of effective charges for each atom and various descriptors of chemical bonds at critical points. This analysis shows that the Nb—O and As/Sb/Bi—O bonds exhibit covalent characteristics, whereas the Ba—O and Ba—As/Sb/Bi bonds are ionic in nature. Analysis of the spectral responses of the examined materials to incident electromagnetic radiation indicates that these compounds exhibit significant absorption in the ultraviolet spectrum and possess a high refractive index in the visible light spectrum.

CRediT authorship contribution statement

Saber Saad Essaoud: Writing – original draft, Methodology, Investigation, Formal analysis, Data curation, Conceptualization. **Missoum Radjai:** Writing – original draft, Validation, Data curation, Conceptualization. **Abdelmadjid Bouhemadou:** Writing – review & editing, Visualization, Validation, Supervision, Software, Resources, Formal analysis, Conceptualization. **Mohammed Elamin Ketfi:** Validation, Supervision, Formal analysis, Conceptualization. **Djamel Allali:** Writing – original draft, Supervision, Conceptualization.

Declaration of competing interest

The authors declare that they have no known competing financial interests or personal relationships that could have appeared to influence the work reported in this paper.

Data availability

Data will be made available on request.

References

[1] I.E. Castelli, K.S. Thygesen, K.W. Jacobsen, Calculated optical absorption of different perovskite phases, J. Mater. Chem. A 3 (2015) 12343–12349.

[2] R. Mguedla, A. Ben Jazia Kharrat, S. Kammoun, K. Khirouni, W. Boujelben, Optical studies of multiferroic HoCrO3 perovskite compound for optoelectronic device applications, Opt. Mater. 119 (2021) 111311, https://doi.org/10.1016/j.optmat.2021.111311.

[3] S. Ravi, High Curie temperature and room temperature magnetoresistance in Pr2FeCrO6 material for spintronics applications, Mater. Lett. 278 (2020) 128448, https://doi.org/10.1016/j.matlet.2020.128448.

[4] H. Roozbahani, S. Maghsoodi, B. Raei, A.S. Kootenaei, Z. Azizi, Effects of catalyst preparation methods on the performance of La2MMnO6 (M = Co, Ni) double perovskites in catalytic combustion of propane, Korean J. Chem. Eng. 39 (2022) 586–595, https://doi.org/10.1007/s11814-021-0930-1.

[5] F. Li, J. Tang, Q. Ke, Y. Guo, M.N. Ha, C. Wan, Z. Lei, J. Gu, Q. Ling, V.N. Nguyen, W. Zhan, Investigation into enhanced catalytic performance for epoxidation of styrene over $LaSrCo_xFe_{2-x}O_6$ double perovskites: the role of singlet oxygen species promoted by the photothermal effect, ACS Catal. 11 (2021) 11855–11866, https://doi.org/10.1021/acscatal.1c03164.

[6] Q. Mahmood, M. Hassan, N. Yousaf, A.A. AlObaid, T.I. Al-Muhimeed, M. Morsi, H. Albalawi, O.A. Alamri, Study of lead-free double perovskites halides Cs2TiCl6, and Cs2TiBr6 for optoelectronics, and thermoelectric applications, Mater. Sci. Semicond. Process. 137 (2022) 106180, https://doi.org/10.1016/j.mssp.2021.106180.

[7] Z. Zhang, Q. Sun, Y. Lu, F. Lu, X. Mu, S.-H. Wei, M. Sui, Hydrogenated Cs2AgBiBr6 for significantly improved efficiency of lead-free inorganic double perovskite solar cell, Nat. Commun. 13 (2022) 3397, https://doi.org/10.1038/s41467-022-31016-w.

[8] C. Wu, Q. Zhang, Y. Liu, W. Luo, X. Guo, Z. Huang, H. Ting, W. Sun, X. Zhong, S. Wei, S. Wang, Z. Chen, L. Xiao, The dawn of lead-free perovskite solar cell: highly stable double perovskite $Cs_2AgBiBr_6$ film, Adv. Sci. 5 (2018) 1700759, https://doi.org/10.1002/advs.201700759.

[9] B.K. Bareth, M.N. Tripathi, R. Maravi, High photovoltaic performance of lead-free Cs2AgInCl6-xBrx perovskite solar cell using DFT and SCAPS-1D simulations, Mater. Today Commun. 39 (2024) 108618, https://doi.org/10.1016/j.mtcomm.2024.108618.

[10] K. Li, S. Li, W. Zhang, Z. Shi, D. Wu, X. Chen, P. Lin, Y. Tian, X. Li, Highly-efficient and stable photocatalytic activity of lead-free Cs2AgInCl6 double perovskite for organic pollutant degradation, J. Colloid Interface Sci. 596 (2021) 376–383, https://doi.org/10.1016/j.jcis.2021.03.144.

[11] A. Bibi, I. Lee, Y. Nah, O. Allam, H. Kim, L.N. Quan, J. Tang, A. Walsh, S.S. Jang, E. H. Sargent, D.H. Kim, Lead-free halide double perovskites: toward stable and sustainable optoelectronic devices, Mater. Today 49 (2021) 123–144, https://doi.org/10.1016/j.mattod.2020.11.026.

[12] P. Sikarwar, I.T. Koneri, T. Appadurai, A.K. Chandiran, Highly efficient photoelectrochemical water oxidation using Cs 2 Ag M Cl 6 (M = In , Bi , Sb) halide double perovskites, Phys. Rev. Appl. 19 (2023) 044083, https://doi.org/10.1103/PhysRevApplied.19.044083.

[13] W. Zheng, X. Gan, D. Du, Y. Wang, S. Dai, L. Guo, H. Liu, First principle study of cesium-based lead-free halide double perovskites, J. Wuhan Univ. Technol.-Mater. Sci. Ed. 38 (2023) 520–529, https://doi.org/10.1007/s11595-023-2727-z.

[14] F. Liu, Structural and optical properties of highly emitting lead-free double perovskites, 2022. <https://iris.unica.it/handle/11584/333072> (Accessed August 26, 2024).

[15] M. Bibes, A. Barthelemy, Oxide spintronics, IEEE Trans. Electron Devices 54 (2007) 1003–1023.

[16] A. Erb, J.B. Philipp, R. Gross, Spin Dependent Transport in the Double Perovskite A2CrWO6 (A= Ca, Sr, Ba), Annu. Rep. Jahresber. (n.d.) 55.

[17] Y. Zhai, J. Qiao, G. Huo, S. Han, Synthesis, magnetic and electrical transport properties of magnetoresistance material Sr2FeMoO6 by microwave sintering, J. Magn. Magn. Mater. 324 (2012) 2006–2010.

[18] C. LI, Mechanically activated synthesis and magnetoresistive behavior of double perovskite Sr2FeMoO6, 2006. <https://core.ac.uk/download/pdf/48645809.pdf> (Accessed August 26, 2024).

[19] D.D. Sarma, E.V. Sampathkumaran, S. Ray, R. Nagarajan, S. Majumdar, A. Kumar, G. Nalini, T.G. Row, Magnetoresistance in ordered and disordered double perovskite oxide, Sr_2FeMoO_6, Solid State Commun. 114 (2000) 465–468.

[20] S.K. Giri, T.K. Nath, Exchange bias effect in nanostructured magnetic oxides, J. Nanosci. Nanotechnol. 14 (2014) 1209–1230.

[21] P. Singh, Magnetic properties of some pyrochlore and double perovskite systems, PhD Thesis, Accessed August 26, 2024, IIT (BHU), Varanasi, 2020.

[22] H. Sakuma, T. Taniyama, Y. Kitamoto, Y. Yamazaki, Cation order and magnetic properties of double perovskite Sr_2FeMoO_6, J. Appl. Phys. 93 (2003) 2816–2819.

[23] X. Xi, J. Liu, Y. Fan, L. Wang, J. Li, M. Li, J.-L. Luo, X.-Z. Fu, Reducing dp band coupling to enhance CO_2 electrocatalytic activity by Mg-doping in Sr2FeMoO6-δ double perovskite for high performance solid oxide electrolysis cells, Nano Energy 82 (2021) 105707.

[24] H. Chang, M. García-Hernández, M. Retuerto, J.A. Alonso, Co-doped Sr 2 FeMoO 6 double perovskites: a plausible scenario for phase segregation, PhysRevB 73 (2006) 104417, https://doi.org/10.1103/PhysRevB.73.104417.

[25] J.J. Alvarado-Flores, R. Mondragón-Sánchez, M.L. Ávalos-Rodríguez, J.V. Alcaraz-Vera, J.G. Rutiaga-Quiñones, S.J. Guevara-Martínez, Synthesis, characterization and kinetic study of the Sr2FeMoO6-δ double perovskite: new findings on the calcination of one of its precursors, Int. J. Hydrog. Energy 46 (2021) 26185–26196.

[26] T. Poudel, Study of Novel Metal Oxide Semiconductor Photoanodes for Photoelectrochemical Water Splitting Applications, The University of Toledo, 2019. <https://search.proquest.com/openview/608e511242e0ef34b3fe8b01c6a2b164/1?pq-origsite=gscholar&cbl=18750&diss=y> (Accessed August 26, 2024).

[27] S. Sâad Essaoud, S.M. Al Azar, A.A. Mousa, A.Y. Al-Reyahi, DFT-Based investigation of electronic-structure, magnetic and thermoelectric properties of Dy2CoMnO6 double perovskite, Phys. Scr. (2023).

[28] N. Al-Aqtash, A.Y. Al-Reyahi, S. Al Azar, S.S. Essaoud, M. Maghrabi, A. Mufleh, M. E. Ketfi, K. Berarma, An ab-initio study on the physical properties of double perovskite Cs2AgXBr6 (X = S, Te, Se), Mater. Today Commun. 38 (2024) 108222, https://doi.org/10.1016/j.mtcomm.2024.108222.

[29] N.A. Aqtash, S.M. Al Azar, A.Y. Al-Reyahi, A. Mufleh, M. Maghrabi, S.S. Essaoud, K. Berarma, A.A. Mousa, First-principles calculations to investigate structural, mechanical, electronic, optical, and thermoelectric properties of novel cubic double Perovskites X2AgBiBr6 (X= Li, Na, K, Rb, Cs) for optoelectronic devices, Mol. Simul. (2023) 1–12.

[30] K. Assiouan, A. Marjaoui, J.E. Khamkhami, M. Zanouni, H. Ziani, A. Bouchrit, A. Achahbar, Theoretical investigation of Rb2AuBiX6 (X= Br, cl, F) double perovskite for thermoelectric and optoelectronic applications, J. Phys. Chem. Solids (2024).

[31] Y. Zhang, Y. Na, W. Hao, T. Gottschall, L. Li, Enhanced cryogenic magnetocaloric effect from 4f-3d exchange interaction in B-site ordered Gd2CuTiO6 double perovskite oxide, Adv. Funct. Mater. N/a (2024) 2409061, https://doi.org/10.1002/adfm.202409061.

[32] M.E. Ketfi, S.S. Essaoud, S.M. Al Azar, A.Y. Al-Reyahi, A.A. Mousa, N. Al-Aqtash, Mechanical, magneto-electronic and thermoelectric properties of Ba2MgReO6 and Ba2YMoO6 based cubic double perovskites: an ab initio study, Phys. Scr. 99 (2023) 015908, https://doi.org/10.1088/1402-4896/ad1021.

[33] R.P. Borges, R.M. Thomas, C. Cullinan, J.M.D. Coey, R. Suryanarayanan, L. Ben-Dor, L. Pinsard-Gaudart, A. Revcolevschi, Magnetic properties of the double perovskites A $_2$ $FeMoO_6$; A = Ca, Sr, Ba, J. Phys. Condens. Matter 11 (1999) L445–L450, https://doi.org/10.1088/0953-8984/11/40/104.

[34] S. Saad Essaoud, M.E. Ketfi, S. Al Azar, A.Y. Al-Reyahi, A. Mufleh, Computational study of structural parameters, magnetic properties, half metallicity, and linear optical characteristics of transition-metal oxide double perovskites: Ba2MnReO6, Ba2NiReO6, and Sr2MnReO6, Indian J. Phys. (2024), https://doi.org/10.1007/s12648-024-03264-7.

[35] M. Ullah, S.A. Khan, G. Murtaza, R. Khenata, N. Ullah, S.B. Omran, Electronic, thermoelectric and magnetic properties of La2NiMnO6 and La2CoMnO6, J. Magn. Magn. Mater. 377 (2015) 197–203.

[36] M. Rani, P.K. Kamlesh, S. Kumawat, U. Rani, G. Arora, A.S. Verma, Rare earth-based oxides double perovskites A2NiMnO6 (A= La and Gd): applications in magneto-caloric, photo-catalytic and thermoelectric devices, Phys. B Condens. Matter 680 (2024) 415645.

[37] T. Maiti, M. Saxena, P. Roy, Double perovskite (Sr2B′ B ″O6) oxides for high-temperature thermoelectric power generation—a review, J. Mater. Res. 34 (2019) 107–125.

[38] I.P. Muthuselvam, R.N. Bhowmik, A. Poddar, La Doped Disorder in La x Ca 2- x FeMoO 6 Ferrimagnet: Magnetic and Thermoelectric Study, in: AIP Conf. Proc., American Institute of Physics, 2011, pp. 260–263. <https://pubs.aip.org/aip/acp/article-abstract/1347/1/260/846816> (Accessed July 22, 2024).

[39] T. Sugahara, N. Van Nong, M. Ohtaki, Structure and thermoelectric properties of $Ca_{2-x}Sr_xFeMoO_6$ ($0 \leq x \leq 0.3$) double-perovskite oxides, Mater. Chem. Phys. 133 (2012) 630–634.

[40] A. Oba, K. Kamishima, K. Kakizaki, N. Hiratsuka, Substitution effect on thermoelectric properties of double Perovskite Sr_2FeMoO_6, Trans. Mater. Res. Soc. Jpn. 37 (2012) 267–270.

[41] Y. Yutoh, M. Yamamoto, H. Kuboya, S. Sugihara, H. Yamauchi, First-principles simulation of electric and magnetic properties of Sr2FeMoO6 and analysis of its thermoelectric properties, Electron. Commun. Jpn. Part II Electron. 88 (2005) 11–18, https://doi.org/10.1002/ecjb.20111.

[42] S. Sugihara, M. Ymamoto, Y. Yutoh, H. Kuboya, H. Yamauchi, New thermoelectric oxide and electronic structures, in: Proc. ICT03 22nd Int. Conf. Thermoelectr. IEEE Cat No 03TH8726, IEEE, 2003, pp. 175–179. <https://ieeexplore.ieee.org/abstract/document/1287477/> (Accessed July 22, 2024).

[43] P. Giannozzi, S. Baroni, N. Bonini, M. Calandra, R. Car, C. Cavazzoni, D. Ceresoli, G.L. Chiarotti, M. Cococcioni, I. Dabo, QUANTUM ESPRESSO: a modular and open-source software project for quantum simulations of materials, J. Phys. Condens. Matter 21 (2009) 395502.

[44] J.P. Perdew, A. Ruzsinszky, G.I. Csonka, O.A. Vydrov, G.E. Scuseria, L. A. Constantin, X. Zhou, K. Burke, Restoring the density-gradient expansion for exchange in solids and surfaces, Phys. Rev. Lett. 100 (2008) 136406.

[45] P. Blaha, K. Schwarz, F. Tran, R. Laskowski, G.K. Madsen, L.D. Marks, WIEN2k: an APW+ lo program for calculating the properties of solids, J. Chem. Phys. 152 (2020) 074101.

[46] A.D. Becke, E.R. Johnson, A Simple Effective Potential for Exchange, American Institute of Physics, 2006.

[47] A. Otero-de-la-Roza, E.R. Johnson, V. Luaña, Critic2: a program for real-space analysis of quantum chemical interactions in solids, Comput. Phys. Commun. 185 (2014) 1007–1018.

[48] R.F. Bader, H. Essén, The characterization of atomic interactions, J. Chem. Phys. 80 (1984) 1943–1960.

[49] Atoms in Molecules, A Quantum Theory, Oxford University Press, Oxford, New York, 1994.

[50] R.F.W. Bader, T.T. Nguyen-Dang, Y. Tal, A topological theory of molecular structure, Rep. Prog. Phys. 44 (1981) 893.

[51] C.F. Matta, R.J. Boyd, An introduction to the quantum theory of atoms in molecules, Quantum Theory At. Mol Solid State DNA Drug Des. (2007).

[52] M.D. Segall, P.J. Lindan, M. al Probert, C.J. Pickard, P.J. Hasnip, S.J. Clark, M. C. Payne, First-principles simulation: ideas, illustrations and the CASTEP code, J. Phys. Condens. 14 (2002,) 2717.

[53] A. Gherriche, A. Bouhemadou, Y. Al-Douri, S. Binomran, R. Khenata, M. Hadi, Ab initio exploration of the structural, elastic, electronic and optical properties of a new layered perovskite-type oxyfluoride: CsSrNb2O6F, Mater. Sci. Semicond. Process. 131 (2021) 105890, https://doi.org/10.1016/j.mssp.2021.105890.

[54] S.S. Essaoud, S.M. Al Azar, A.A. Mousa, R.S. Masharfe, Characterization of structural, dynamic, optoelectronic, thermodynamic, mechanical and thermoelectric properties of AMgF3 (A= K or Ag) fluoro-perovskites compounds, Phys. Scr. 98 (2023) 035820.

[55] R. Bianchi, G. Gervasio, D. Marabello, Experimental electron density analysis of $Mn_2(CO)_{10}$: metal−metal and metal−ligand bond characterization, Inorg. Chem. 39 (2000) 2360–2366, https://doi.org/10.1021/ic991316e.

[56] S. Al-Essa, S.S. Essaoud, A. Bouhemadou, M.E. Ketfi, S. Maabed, F. Djilani, S. Bin-Omran, M. Radjai, D. Allali, R. Khenata, An ab initio analysis of the electronic, optical, and thermoelectric characteristics of the Zintl phase CsGaSb2, Phys. Scr. 99 (2024) 095996.

[57] G.K. Madsen, D.J. Singh, BoltzTraP, A code for calculating band-structure dependent quantities, Comput. Phys. Commun. 175 (2006) 67–71.

[58] F. Hamioud, A.A. Mubarak, Structural, elastic and optoelectronic properties of the hydrogen based perovskite compounds: ab-initio study, Chin. J. Phys. 56 (2018) 1–9.

[59] M.M. Hossain, First-principles study on the structural, elastic, electronic and optical properties of $LiNbO_3$, Accessed August 25, 2024, Heliyon 5 (2019), https://www.cell.com/heliyon/fulltext/S2405-8440(18)36460-0.

[60] S.C. Mouna, M. Radjai, A. Bouhemadou, D. Houatis, D. Allali, S.S. Essaoud, S. Bin-Omran, Structural, elastic, and thermodynamic properties of BaXCl3 (X= Li, Na) perovskites under pressure effect: ab initio exploration, Phys. Scr. 98 (2023) 065949.

[61] D.R. Penn, Wave-number-dependent dielectric function of semiconductors, Phys. Rev. 128 (1962) 2093.

[62] M.I. Hussain, R.A. Khalil, F. Hussain, M. Imran, A.M. Rana, S. Kim, Investigations of structural, electronic and optical properties of TM-GaO3 (TM= Sc, Ti, Ag) perovskite oxides for optoelectronic applications: a first principles study, Mater. Res. Exp. 7 (2020) 015906.

[63] H. Zitouni, N. Tahiri, O. El Bounagui, H. Ez-Zahraouy, How the strain effects decreases the band gap energy in the $CsPbX_3$ perovskite compounds? Phase Transit. 93 (2020) 455–469, https://doi.org/10.1080/01411594.2020.1746964.